Assessing T cell differentiation at the single-cell level

Gerlach, C.

Citation

Gerlach, C. (2012, January 17). *Assessing T cell differentiation at the single-cell level*. Retrieved from https://hdl.handle.net/1887/18361

8

THE CD8+ T CELL RESPONSE TO INFECTION IS DOMINATED BY THE PROGENY OF A FEW NAÏVE T CELLS

Carmen Gerlach[1], Jan Rohr[1], Nienke van Rooij[1], Arno Velds[2], Leïla Perié[1,3], Michael Hauptmann[4], Shalin H. Naik[1], Rob J. de Boer[3] and Ton N.M. Schumacher[1]

[1]Division of Immunology, [2]Deep sequencing Facility and [4]Bioinformatics and Statistics Group, Division of Molecular Biology, The Netherlands Cancer Institute, Department of Immunology, Amsterdam, the Netherlands; [3]Department of Theoretical Biology, Utrecht University, Utrecht, the Netherlands

Following infection, antigen-specific CD8$^+$ T cell numbers increase dramatically. Analysis of antigen-specific T cell responses at the bulk cell level has provided insight into the average number of cell divisions that T cells undergo upon activation. However, it is unclear whether all naïve T cells of a given affinity for antigen produce equal numbers of progeny, or whether the total effector T cell pool is predominantly created by the output of few. To quantify how many daughter cells individual naïve T cells produce, we have generated naïve OT-I T cells harboring unique genetic tags (barcodes) and have measured the number of progeny per labeled cell by second-generation sequencing of barcode sequences after infection. Our data reveal that upon bacterial or viral infection, individual OT-I T cells that are recruited into the response produce highly variable numbers of daughter cells, and that this strong disparity in output is established during the first phase of infection. Importantly, the numerical dominance of the output of a small number of recruited cells becomes increasingly prominent when either CD80/CD86-mediated costimulation is disrupted, when T cell responses are induced by low affinity antigens or when pathogen load is low. These data indicate that in particular in situations in which T cell activation signals are limited, antigen-specific CD8$^+$ T cell responses are largely composed by the progeny of only a few cells.

INTRODUCTION

The CD8^{+} T cell pool is shaped by pathogen encounter. The naïve CD8^{+} T cell repertoire contains some ~80-1200 cells that recognize a given epitope[1,2]. Following infection, the majority of these antigen-specific CD8^{+} T cells are recruited into the immune response[3] and collectively these cells produce up to 10[7] antigen-specific cells as progeny[2,4,5]. Based on this type of quantification of T cell responses at the bulk cell level, it has been estimated that CD8^{+} T cells divide on average 14 times in response to LCMV infection[2,5]. An untested assumption in such quantifications is however that the clonal burst generated by each naïve T cell (i.e. the number of progeny) is roughly equal.

From CFSE dilution experiments it is apparent that naïve T cells - even when expressing the same T cell receptor – do not all complete their first division at the same time[6-8]. Likewise, asynchronous initiation of cell division by antigen specific T cells is suggested by imaging studies on explanted lymph nodes, in which generally only one of the antigen-specific T cells within the imaging field entered mitosis during a defined time frame[9,10]. However, whether asynchronous initiation of proliferation or other variables such as division and death rates would influence the progeny size of T cells with an identical antigen specificity remains unclear.

To reveal to what extent individual cells (in this case naïve antigen-specific T lymphocytes) differ in the number of progeny they produce it is essential to assign all the cells that are produced during an immune response to specific 'families', in which all the daughters from a single naïve T cell form a separate family. Over the past years, two fundamentally different technologies have been developed for such analysis of cellular descent[11]. First, cellular kinship can be revealed by the continuous tracing of cells by microscopy, and in recent work, the behavior of individual CpG-stimulated B cells and their progeny have been tracked *in vitro* by video microscopy[12]. These analyses have shown the existence of some degree of heritability in B cell division and death rates, with times to next division and times to death being more similar amongst siblings than between randomly picked cells within the population. The use of continuous tracing to reveal cellular kinship in vivo is presently limited to periods of hours and restricted to cases in which progeny stays local. However, T cell responses develop over periods of days and T cell progeny is not locally confined. Therefore, other technologies are required to map *in vivo* cell fate. Over the past years, two strategies have been developed towards this goal. Busch and colleagues have pioneered the transfer of individual T cells into recipient mice, thereby allowing fate mapping by allotype marking[13]. Alternatively, we have developed a technology to endow naïve T cells with unique genetic tags, which allows one to distinguish the progeny of individual cells on the basis of the genetic tag ('barcode') they carry. [3,11,14,15]. Specifically, through retroviral transduction of thymocytes[15] with a library of barcodes, a pool of naïve T cells, each carrying a unique genetic tag, can be created. As these barcodes are transferred to all progeny of the respective naïve T cell, all members of a given T cell family are marked with an identical barcode sequence.

8

Here we have combined this barcode labeling system with second-generation sequencing[16-19] to quantify the output of individual naïve T cells under different conditions of infection.

The data obtained reveal that within the population of responding T cells, individual T cell family sizes are highly variable, in spite of the fact that all tracked T cells possess the same antigen specificity. As a result of this, few T cell families dominate the overall response, with ~20% of the responding naïve T cells contributing to 90% of the total response magnitude. The dominance by a selected number of T cell families is established during the early phase of infection and becomes more pronounced in situations of weak T cell stimulation.

RESULTS

Quantification of T cell family size by second-generation sequencing

The development of the cellular barcoding technology[3,11,14,15] has made it possible to track the fate of several hundred individual naïve T cells and their daughters *in vivo*, as all progeny of the same naïve T cell precursor can be identified by an identical and unique genetic marker – the barcode. Previously, the representation of different T cell families within subpopulations of responding T cells (e.g. effector and memory T cell populations[15,20]) was determined by microarray hybridization. This readout system is well suited to detect the relative abundance of T cell families in two populations of interest by a ratiometric measurement. However, as the system is not calibrated, it is not possible to infer absolute T cell family sizes from the data obtained by this technology.

In order to accurately quantify the sizes of genetically tagged (T) cell families, we therefore developed a novel barcode-readout system that is based on second-generation sequencing. As second-generation sequencing (also referred to as next-generation or deep sequencing) yields millions of individual sequences within a single reaction[16-19], it has the potential to provide a highly quantitative measure of the abundance of individual DNA barcodes within a cell population, provided obviously that no significant bias is introduced during barcode recovery or amplification.

To first test to what extent barcode quantification by second-generation sequencing is able to accurately describe the frequency of cells with that specific tag within a cell population of interest, we transduced a human T cell line with the barcode library and generated 20 clones that each harbor a unique barcode. Subsequently, the clones were mixed in varying amounts and barcode frequencies within this mixed cell population were determined by second-generation sequencing. Comparison of these data with the input cell numbers per clone demonstrated that deviation from the expected ratio of 1 was small (max 1.87; min 0.33) for all clones constituting >0.2% of the total population (Fig. S1A). Thus, quantification of barcodes by deep sequencing can be used to describe the composition of cell populations over a large dynamic range (Fig. S1B).

OT-I T cell responses are dominated by the progeny of few naïve T cells

Having validated the use of deep sequencing for barcode quantification, we determined the extent to which the progeny of individual T cells that all share the same T cell receptor contribute to the overall ('bulk') response of these cells. To this purpose, naïve barcode-labeled (GFP+) TCR-transgenic OT-I T cells were generated by thymocte transduction, and injected intra-thymically to allow for their differentiation into mature naïve T cells[15]. Approximately 800 barcode-labeled naïve OT-I T cells were transferred into B6 recipients, which were then infected with a recombinant *Listeria monocytogenes* strain expressing the SIINFEKL epitope (LM-OVA) that is recognized by the OT-I TCR. Seven days later, spleen and lymph nodes were harvested and the abundance of each barcode was quantified by second-generation sequencing. In addition, the overall OT-I T cell response magnitude was determined by flow cytometry.

To assess whether barcode quantification was reproducible, amplification and sequencing was performed in parallel on two independent half-samples taken from each recipient mouse, and read counts (reflecting sequence abundance) of all
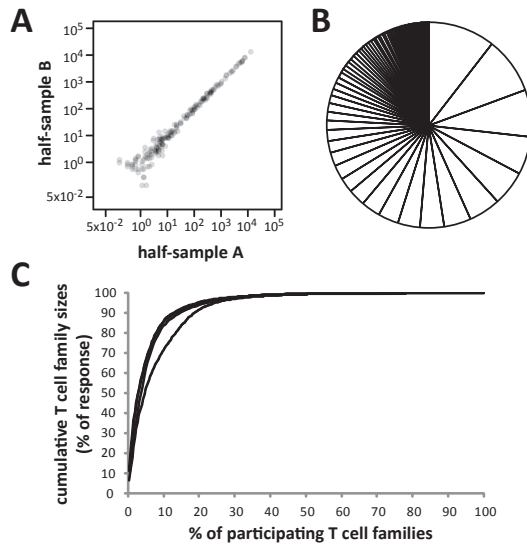
8

Figure 1: T cell responses are dominated by the progeny of few naïve T cells. ~800 naïve, barcode-labeled OT-I T cells were transferred into 4 B6 recipient mice that were infected with LM-OVA the next day. 7 days after infection, spleen and LNs were harvested and OT-I T cell family sizes were quantified. (**A**) Relative barcode abundances (# of reads out of 100'000) in two independent half-samples (sample A and B) of the same cell population of one representative mouse. Each dot corresponds to one barcode. A distribution control is provided in Fig. S2A. (**B**) Contribution of participating OT-I T cell families to the magnitude of the overall response. Each piece of the pie represents the average size of the first to nth OT-I family for 4 mice. (**C**) Cumulative OT-I family sizes depicted as a function of the percentage of OT-I families participating in the response. Each line represents one mouse. Data are representative of 9 independent experiments.

barcodes were compared between the two half-samples (Fig. 1A). In all experiments, the prevalence of all barcodes identified within a given cell population was highly reproducible in these replicate measurements. Furthermore, overlap between barcodes recovered from different mice was low and for the low proportion of shared barcodes signal intensity was uncorrelated (Fig. S2A). This rules out sample contamination with barcodes originating from other samples as a confounding factor. Collectively, these data indicate that barcode deep sequencing forms a reproducible measure of barcode prevalence within a responding T cell population.

Interestingly, analysis of the relative abundance of the distinct barcode sequences detected within an antigen-specific T cell response indicated that the size of different OT-I families was highly diverse (Fig. 1A-C and S2B). Of the greater than 200 OT-I T cell families detected in each mouse of this experiment, the largest family constituted on average 10 percent of the total OT-I response (Fig. S2B, left plot; absolute family size >80,000 cells, right plot). In comparison, the median T cell family size was ~500-fold lower, at 0.015% of the overall response. Importantly, the smallest detected OT-I families were composed of ~4 cells, demonstrating that this assay system measured the progeny of OT-I T cells that had been recruited into the response. Thus, even though all tracked naïve T cells expressed the same TCR, there was a striking disparity in the amount of offspring they generated: On average, 50% of the total antigen-specific T cell response was formed by the progeny of just 3.5% of the activated OT-I cells, and 15% of the recruited T cells produced 90% of the effector T cell population (Fig. 1C).

Of the 2 display formats utilized to represent T cell family sizes (Fig. 1B+C), the first is expected to be sensitive to the amount of OT-I T cells that are recruited into the response, while the second is not. To formally test this, we transferred different numbers of naïve barcode-labeled OT-I cells into B6 recipients and quantified barcode abundance upon LM-OVA infection. As expected, the overall OT-I response magnitude was higher and a larger number of OT-I families participated in the response when a larger number of OT-I cells was transferred (Fig. S3B+C). Importantly, family sizes were highly variable in both groups (Fig. 2A-C and S3D). Plotting of the data demonstrated that - according to expectation - pie chart representations are influenced by the number of T cell families participating in the response, whereas saturation curves that plot the cumulative OT-I response magnitude as a function of the percentage of the total number of participating OT-I families are not. (Fig. 2B+C). Thus, the former type of data presentation is useful to reveal how the overall composition of a responding T cell population is influenced by variation in the conditions of infection (see below), while the latter specifically depicts the level of disparity in family sizes independent of the number of T cell families that participated.

Thus, the above data indicate that in response to LM-OVA infection, the progeny of a few T cells comprises the bulk of the overall OT-I T cell response. This numerical dominance by a minority of OT-I families was also observed in response to OVA-expressing influenza infection (Fig. 2D-F). Furthermore, this dominance was not
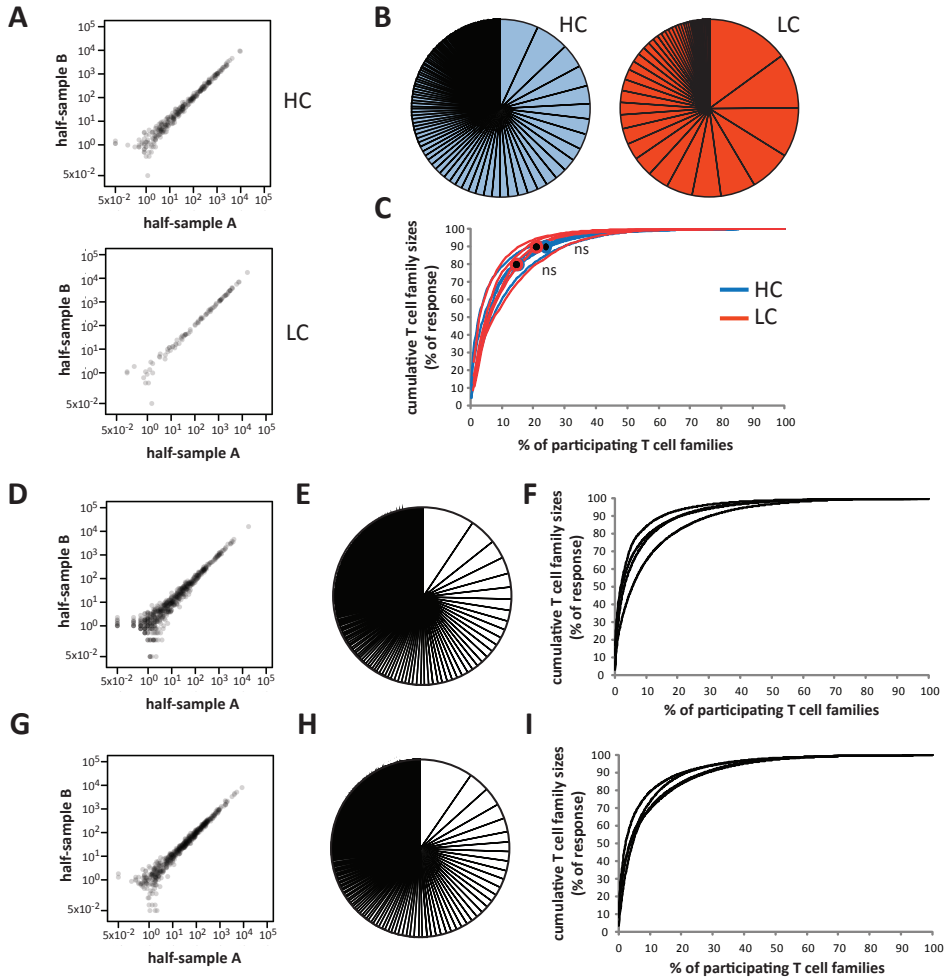
Figure 2: T cell family size disparity in OT-I rag2⁻/⁻ T cell responses and as a function of naïve T cell frequency. (A-C) 760 (high cell numbers; HC) or 190 (low cell numbers; LC) naïve, barcode-labeled OT-I T cells were transferred into 5 B6 recipient mice that were infected with LM-OVA the next day. 7 days after infection, spleen and LNs were harvested and OT-I T cell family sizes were quantified. Representative distribution controls are provided in Fig. S3A. **(D-F)** ~400 naïve, barcode-labeled OT-I T cells were transferred into 4 B6 recipient mice that were infected with Influenza-OVA the next day. 9 days after infection OT-I T cell family sizes were quantified from spleen cells. A distribution control is provided in Fig. S3E. **(G-I)** ~1000 naïve, barcode-labeled OT-I, rag2⁻/⁻ T cells were transferred into 4 B6 recipient mice that were infected with LM-OVA the next day. 7 days after infection, spleen and LNs were harvested and OT-I T cell family sizes were quantified. A distribution control is provided in Fig. S3F. (**A, D, G**) Relative barcode abundances (# of reads out of 100'000) in two independent half-samples (sample A and B) of the same cell population of one representative mouse. Each dot corresponds to one barcode. (**B, E, H**) Contribution of participating OT-I T cell families to the magnitude of the overall response. Each piece of the pie represents the average size of the first to nth OT-I family for 4 mice. (**C, F, I**) Cumulative OT-I family sizes depicted as a function of the percentage of OT-I families participating in the response. Each line represents one mouse. Circles represent the average % of participating T cell families per group to constitute 80% or 90% of the total response. (**C**) Differences in the fraction of participating T cell families constituting 80% (P=0.8413) and 90% (P=0.3095) are non-significant (ns).

related to rearrangement of the endogenous TCR loci in some of the OT-I T cells, as LM-OVA-induced responses of OT-I rag2^{-/-} T cells were also largely composed by the output of a small number of cells (Fig 2G-I).

Once a large family – always a large family

To test at what time post infection the disparity in OT-I family sizes takes shape, we transferred barcode-labeled naïve OT-I T cells into B6 recipient mice and quantified family sizes in spleen and lymph nodes at day 5, 6, 7 or 8 after LM-OVA infection. As expected, the total number of OT-I T cells increased dramatically from day 5 to 8 (peak of response), with the largest (31-fold) expansion of the population occurring between day 5 and 6 (Fig S4B). Barcodes could be quantified reproducibly even from the small numbers of barcode-labeled cells obtained early after infection (Fig 3A) and the number of responding OT-I families was comparable at all days (Fig. S4C). Importantly, differences in family sizes were observed already at day 5, and the magnitude of these differences did not significantly change to day 8 (Fig 3B-C and S4D). This experiment demonstrates that a marked disparity in the clonal burst generated by individual T cells is already evident as early as day 5 post-infection, indicating that any factor influencing T cell family size must have acted before this time.

To address whether the T cell families that contributed most to the acute antigen-specific T cell response also remained dominant after the infection has waned, we harvested spleen cells from the same mice at two different time points after LM-OVA infection and compared OT-I T cell family sizes between these two samples. At both days, barcodes were reproducibly quantified (Fig. 4A). When the size of each OT-I family was compared between day 8 and 32, it was apparent that even though the exact order of dominance was not maintained, all families that were large at day 8 remained large 3 weeks later, intermediate families were still intermediate in size and small families remained small (Fig. 4B). Together, these kinetic data demonstrate that differences in OT-I T cell family sizes are present already early on during an antigen-specific T cell response and are maintained thereafter.

CD80/ CD86-mediated costimulation influences the disparity in T cell family sizes

The above data are consistent with a model in which the magnitude of the CD8^{+} T cell clonal burst is determined early after or during T cell activation. To determine whether the conditions under which T cell activation takes place could influence the observed disparity in T cell family sizes, we set out to create a setting in which T cell activating signals were reduced. For this purpose, disruption of CD80/86 mediated costimulation was selected, as the absence of CD80/86 is known to reduce T cell response magnitude substantially and signaling through CD28 is thought to function as a signal amplifier for weak signals received by the TCR[21]. Thus, in case T cell family size disparity would be influenced by the strength of the T cell activating signal, such a disparity may potentially be enhanced in a CD80/86 deficient setting.

To assess the effect of CD80/86 mediated costimulation on T cell family dominance, we transferred barcode-labeled naïve OT-I T cells into control B6 and
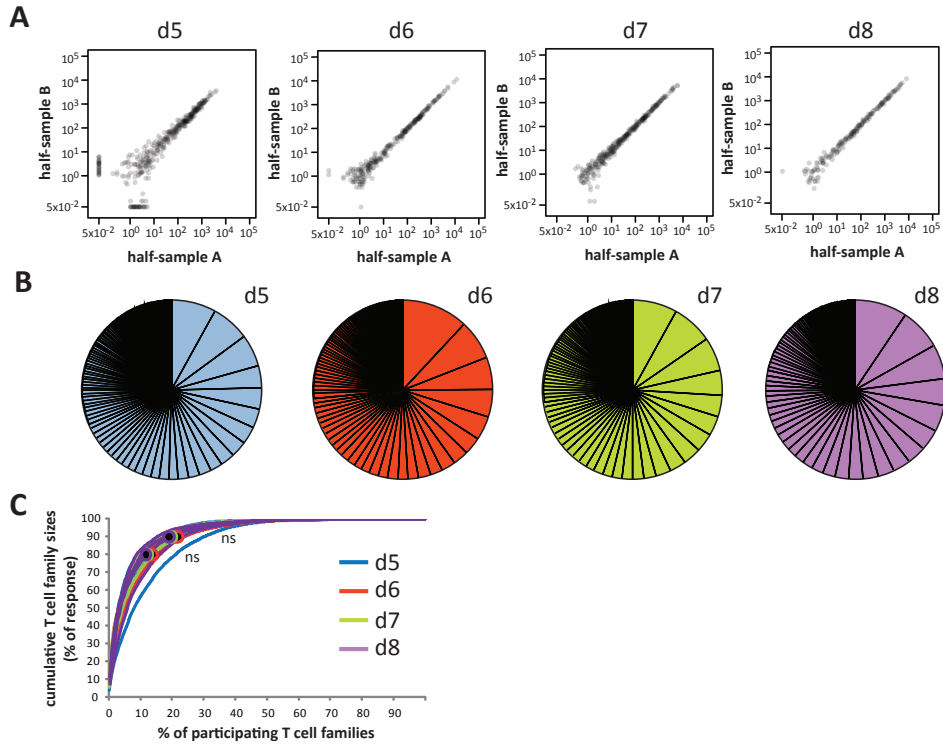
8

Figure 3: Differences in T cell family sizes are already observed early during the response. ~1600 naïve, barcode-labeled OT-I T cells were transferred into 16 B6 recipient mice that were infected with LM-OVA the next day. At day 5, 6, 7 and 8 after infection, spleen and LNs were harvested from 4 mice and OT-I T cell family sizes were quantified. (**A**) Relative barcode abundances (# of reads out of 100'000) in two independent half-samples (sample A and B) of the same cell population of one representative mouse. Each dot corresponds to one barcode. A distribution control is provided in Fig. S4A. (**B**) Contribution of participating OT-I T cell families to the magnitude of the overall response. Each piece of the pie represents the average size of the first to nth OT-I family for 4 mice. (**C**) Cumulative OT-I family sizes depicted as a function of the percentage of OT-I families participating in the response. Each line represents one mouse. Circles represent the average % of participating T cell families per group to constitute 80% or 90% of the total response. Differences in the fraction of participating T cell families constituting 80% (P=0.5507) and 90% (P=0.4908) are non-significant (ns). Data are representative of 2 independent experiments.

CD80$^{-/-}$CD86$^{-/-}$ recipients and quantified both the overall response magnitude and individual OT-I family sizes at day 7 post LM-OVA infection.

The overall OT-I T cell response was markedly reduced in CD80$^{-/-}$CD86$^{-/-}$ mice (Fig. S5B) even though the number of participating OT-I families was only somewhat (~1.3-fold) reduced (Fig. S5C). Both in the absence and presence of CD80/CD86-mediated costimulation, individual OT-I family sizes were diverse (Fig. 5A-C and S5D), and as expected from the large difference in overall response magnitudes, the most dominant
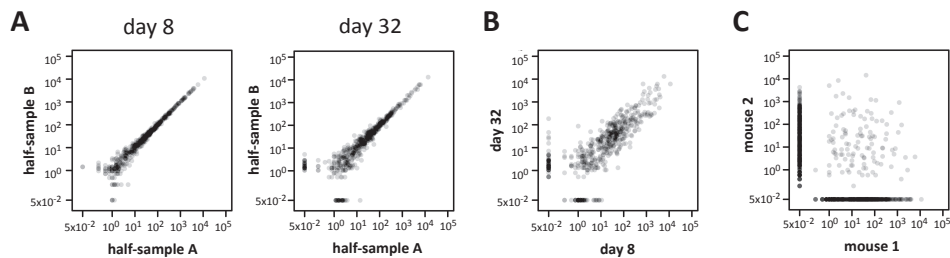
Figure 4: Differences in T cell family sizes are maintained during the response. ~640 naïve, barcode-labeled OT-I T cells were transferred into 4 B6 recipient mice that were infected with LM-OVA the next day. 8 days after infection ¼ of the spleen was isolated by partial splenectomy and the remainder of the spleen was isolated at day 32. OT-I T cell family sizes were quantified from both samples. (**A**) Read numbers per barcode in both half-samples obtained either at day 8 or 32. (**B**) Read numbers per barcode compared between two half-samples obtained at day 8 and day 32. (**C**) Representative distribution control.

OT-I families in the wild-type mice are larger in terms of absolute family members than in the CD80$^{-/-}$CD86$^{-/-}$ recipients (Fig. S5D, right graph). Interestingly, the largest OT-I family in the CD80$^{-/-}$CD86$^{-/-}$ recipients constituted a larger fraction of the total response than the most prevalent family in the wild-type mice (Fig. 5B and S5D, left graph). This is in part a reflection of the slight reduction in OT-I families participating in the response, but primarily the result of a significantly increased disparity in the clonal burst of the T cells that have been recruited: In order to constitute 90% of the total response, on average 33.5 out of 310 families (10.8%) in the knockout mice and 94 out of 387 families (24.3%) in the wildtype mice were required.

Taken together, this experiment shows that in the absence of CD80 and CD86-mediated costimulation, the overall response is dominated by even fewer OT-I T cell families. This occurs both because slightly fewer antigen-specific T cells are recruited into the response and in particular because amongst the families that do participate, the variation in family size is very pronounced.

The dominance of a few T cell families is more pronounced in response to lower affinity antigens and reduced antigen dose

To investigate if weaker T cell stimulation in general results in a more pronounced dominance of a few T cell families, we assessed whether disparity in T cell family sizes is shaped by antigen affinity.

To this purpose, OT-I family sizes were quantified 7 days after infection with *Listeria monocytogenes* strains harboring either the native OT-I ligand SII**N**FEKL (LM-OVA / LM-N4), or the altered peptide ligands SII**Q**FEKL (LM-Q4) or SII**T**FEKL (LM-T4). The latter two are recognized by OT-I T cells with ~18-fold and ~71-fold lower avidity, respectively[22].
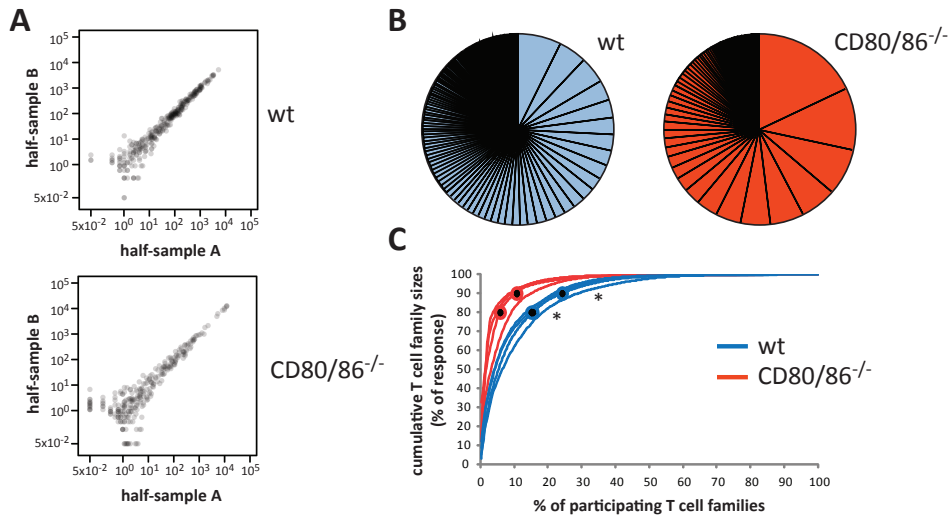
Figure 5: CD80/CD86-mediated costimulation influences the disparity in T cell family sizes. ~800 naïve, barcode-labeled OT-I T cells were transferred into 4 B6 or 4 CD80$^{-/-}$ CD86$^{-/-}$ recipient mice that were infected with LM-OVA the next day. At day 7 after infection OT-I family sizes were quantified from spleen and LN cells. (**A**) Relative barcode abundances (# of reads out of 100'000) in two independent half-samples (sample A and B) of the same cell population of one representative mouse. Each dot corresponds to one barcode. A distribution control is provided in Fig. S5A. (**B**) Contribution of participating OT-I T cell families to the magnitude of the overall response. Each piece of the pie represents the average size of the first to nth OT-I family for 4 mice. (**C**) Cumulative OT-I family sizes depicted as a function of the percentage of OT-I families participating in the response. Each line represents one mouse. Circles represent the average % of participating T cell families per group to constitute 80% or 90% of the total response. Differences in the fraction of participating T cell families constituting 80% (P=0.02857) and 90% (P=0.02857) are significant (*). Data are representative of 2 independent experiments.

Barcode quantification was reproducible (Fig. 6A) and as expected, the overall magnitude of the OT-I responses was markedly reduced in the lower affinity groups (Fig. S6B). Similar to T cell activation in the absence of CD80 and CD86, somewhat fewer OT-I families participated in the responses against the lower affinity antigens (Fig. S6C). In all groups T cell family sizes were diverse (Fig. 6B-C and S6D), however, in the groups stimulated by lower affinity antigens the dominant OT-I families contributed to a larger proportion of the overall response (Fig. 6B and S6D, left plot). Among the OT-I families participating in the response, the fraction of families required to constitute 80% or 90% of the overall response decreased significantly with reduced antigen affinity (Fig. 6C). Thus, the increased dominance of a small number of T cell families upon stimulation with low affinity antigen is due to two factors: a slight reduction (~1.4-fold) in the number of families participating in the response and a significantly larger disparity in family size among the families that do participate.
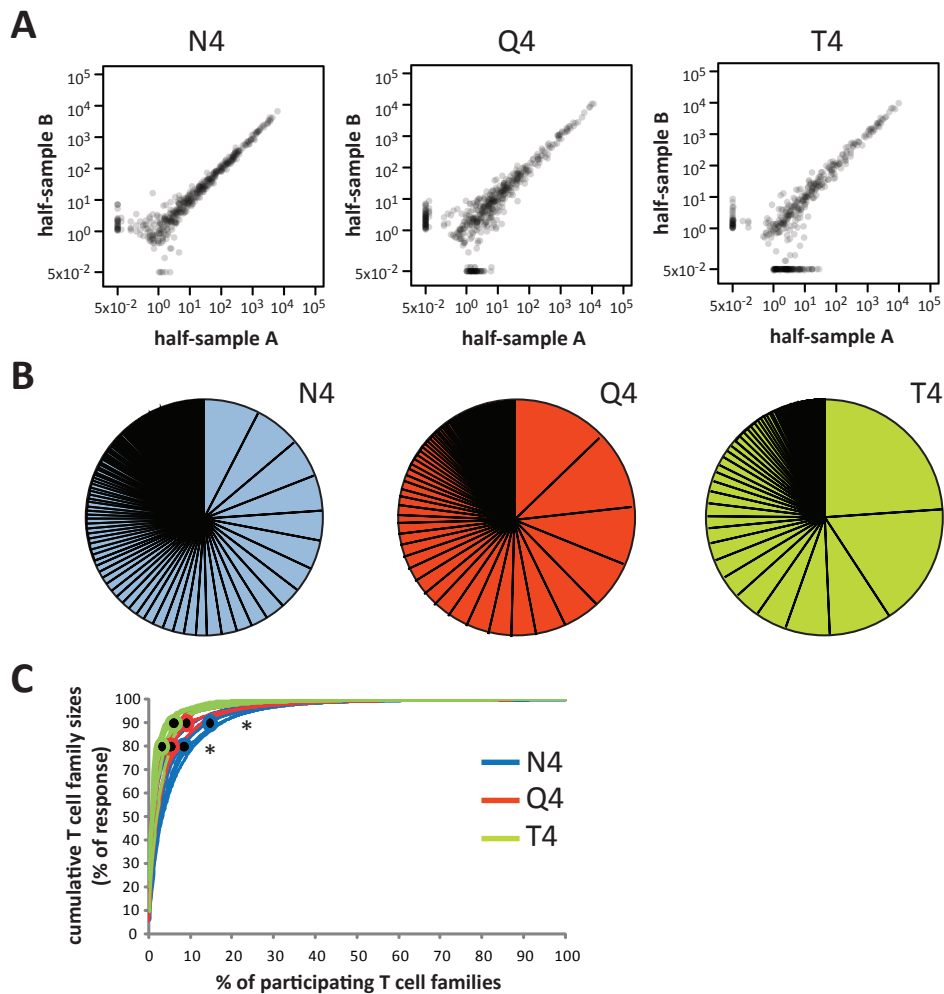
Figure 6: The dominance of a few T cell families is more pronounced in response to lower affinity antigens. ~640 naïve, barcode-labeled OT-I T cells were transferred into 16 B6 recipient mice, of which 5 were infected with LM-N4, 5 with LM-Q4 and 6 with LM-T4 the next day. At day 7 after infection OT-I family sizes were quantified from spleen and LN cells. (**A**) Relative barcode abundances (# of reads out of 100'000) in two independent half-samples (sample A and B) of the same cell population of one representative mouse. Each dot corresponds to one barcode. A distribution control is provided in Fig. S6A. (**B**) Contribution of participating OT-I T cell families to the magnitude of the overall response. Each piece of the pie represents the average size of the first to n^{th} OT-I family for 5-6 mice. (**C**) Cumulative OT-I family sizes depicted as a function of the percentage of OT-I families participating in the response. Each line represents one mouse. Circles represent the average % of participating T cell families per group to constitute 80% or 90% of the total response. The fraction of participating T cell families constituting 80% (P=7.334x10^{-5}) and 90% (P=3.766x10^{-5}) decreases significantly with decreasing antigen affinity (*). Data are representative of 2 independent experiments.

To further investigate the influence of T cell stimulation strength on the disparity of responding T cell family sizes, we quantified OT-I T cell family sizes after infection with different doses of LM-OVA bacteria. The magnitude of the bulk OT-I response was 6-fold lower after infection with the low bacterial dose (Fig. S7B) and in this experiment 2.6-fold fewer OT-I families participated in the response (Fig. S7C). From both groups, barcode quantification was reproducible (Fig. 7A) and family sizes were heterogeneous (Fig. 7B and S7D). Among the participating OT-I families, there was a trend towards a larger disparity in family sizes after low-dose infection. This observation did not reach statistical significance with the group sizes used. To increase the statistical power of the analysis, this experiment will be repeated with larger group sizes and an additional intermediate-dose group.
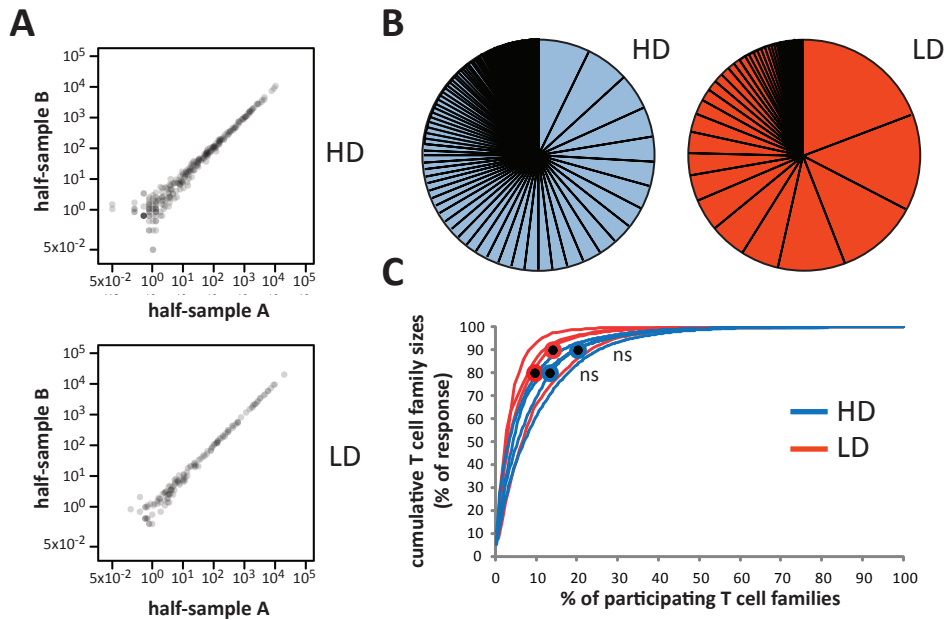

Figure 7: Influence of antigen dose on the disparity in T cell family sizes. ~880 naïve, barcode-labeled OT-I T cells were transferred into 8 B6 recipient mice, of which 4 were infected with 500 CFU LM-OVA (low dose; LD) and 4 with 25'000 CFU (high dose; HD) the next day. At day 7 after infection OT-I family sizes were quantified from spleen and LN cells. (**A**) Relative barcode abundances (# of reads out of 100'000) in two independent half-samples (sample A and B) of the same cell population of one representative mouse. Each dot corresponds to one barcode. A distribution control is provided in Fig. S7A. (**B**) Contribution of participating OT-I T cell families to the magnitude of the overall response. Each piece of the pie represents the average size of the first to n^{th} OT-I family for 4 mice. (**C**) Cumulative OT-I family sizes depicted as a function of the percentage of OT-I families participating in the response. Each line represents one mouse. Circles represent the average % of participating T cell families per group to constitute 80% or 90% of the total response. Differences between groups are non-significant (ns): 80% (P=0.2); 90% (P=0.2).

Together, these experiments demonstrate that OT-I T cell responses to lower affinity antigens are dominated by a smaller number of T cell families than T cell responses induced by high affinity antigen, and suggest that reduced antigen dose may lead to the same effect. Together with the data on the effect of CD80/86 costimulation, these results argue that the strength of the T cell activating signal determines the extent to which T cell responses are biased towards the output of a small number of cells.

DISCUSSION

While it is known that antigen-specific T cell populations expand dramatically upon infection, it is currently unclear whether all naïve T cells of a given affinity for antigen produce equal numbers of progeny. The aim of this study was therefore to quantify the output of individual naïve T cells in response to infection *in vivo*.

After developing a quantitative, second-generation sequencing-based readout system for use in conjuction with cellular barcoding, we demonstrated that individual OT-I T cells produce highly variable numbers of progeny upon OVA-expressing *Listeria monocytogenes* or influenza infection. As a result of this disparity, the total OT-I effector pool is dominated by only a few T cell families. It has previously been shown that T cell responses to infection are predominantly composed of T cells recognizing the antigen with high affinity[23-25]. Here we demonstrate that even within this high affinity repertoire, the progeny of only a minor fraction of the available cells dominates the response.

Two fundamentally different mechanisms could account for the observed disparity in T cell family sizes. First, individual T cell families could have distinct proliferation and/or death rates (collectively referred to as 'propagation rates' here). Second, individual antigen-specific naïve T cells could enter their first division at distinct moments in time and thus start to participate in the response asynchronously.

As we find that the extent of family size disparity does not significantly change after day 5 post infection, we consider it unlikely that stably distinct propagation rates for different T cell families underlie the observed disparity, as this would result in an increased disparity over time. Two more likely explanations for the observed dominance are therefore that I) not all antigen-specific T cells enter their first division at the same time and/or that II) propagation rates are variable between T cell families early after activation, but that this difference levels out before day 5. Using CFSE dilution, we are currently investigating the kinetics by which antigen-specific T cells complete their first division. We will subsequently use these data to mathematically model whether the measured differences in times to first division can explain the observed disparity in T cell family sizes, or whether additional early differences in propagation rates are required to obtain the pattern of T cell family dominance that is observed.

By inducing *in vivo* T cell activation in the absence or presence of CD80 and CD86-mediated costimulation, with antigens of different affinity, or with different antigen doses, we demonstrated that the extent of T cell family size disparity is not fixed, as

it was influenced by the environment in which the cells were stimulated. Conditions providing limited T cell stimulation intensified the disparity in output of the stimulated cells. These data suggest that the level of antigen affinity, antigen dose and CD80/CD86-mediated costimulation influence the variation in times to first division and/or propagation rates of the antigen-specific T cells.

What determines which of the antigen-specific T cells will form a large or a small family? In principle, these could be deterministic or stochastic processes. One could speculate that while all tracked T cells harbor the same TCR specificity, the level of TCR expression is variable. Those T cells with higher TCR density on their surface would recognize the antigen with higher avidity and could therefore initiate proliferation earlier or the stronger trigger they receive would speed up their expansion rate. Likewise, stochastic variation in signaling molecules may influence T cell behavior. As an alternative explanation, family dominance could simply be a matter of which T cell is at the right place at the right moment. As naïve T cell circulate between the secondary lymphoid organs, they are dispersed throughout the body and only a small fraction of the antigen-specific cell population will be close to the site of pathogen entry. It is conceivable that the conditions of antigen presentation and the inflammatory environment will be different for those cells that are already present at the infection site and those that arrive later. Whatever the underlying mechanism, in both cases an environment providing a weaker T cell activating signal can be expected to result in an increased diversity in times to first division and/or propagation rates of the antigen-specific T cells and thereby control T cell family size disparity.

MATERIALS AND METHODS

Mice. C57BL/6 (B6) mice were obtained from Charles River. CD80^{-/-}CD86^{-/-} mice and TCR-transgenic OT-I and OT-I rag2^{-/-} mice were bred and housed in the animal department of the Netherlands Cancer Institute (NKI). All animal experiments were performed in accordance with national guidelines and were approved by the Experimental Animal Committee of the NKI.

Generation and mixing of single-barcode clones. Retroviral supernatants were obtained by transfection of the barcode-library[14] DNA into Phoenix-A packaging cells using FuGENE™6 transfection reagent (Roche Diagnostics). Jurkat cells were transduced by spin-infection with diluted retroviral supernatants to reach a transduction efficiency of 1-2% (at this transduction efficiency, the mean number of barcodes per cell is close to one[14]). One day after transduction, GFP[+] (transduced) cells were sorted as single-cells by FACS. From the clones that grew, genomic DNA was isolated and barcode sequences were amplified and sequenced by second-generation sequencing (as described below) to confirm the presence of one barcode per clone.

To assess how representative barcode quantification by second-generation sequencing is of the barcode abundance in a cell population, different cell numbers of twenty distinct single-barcode clones were mixed. The cell numbers ranged from 10

8

to 5'242'880 cells (2-fold steps), reaching a total of 10'485'750 cells. Genomic DNA was isolated from two of these mixtures and barcode sequences were amplified and sequenced as described below.

Generation and transfer of naïve, barcode-labeled T cells. Total thymocytes isolated from 4-8 weeks old OT-I or OT-I rag2^{-/-} donor mice were transduced with the barcode-library by spin-infection (90min. 2000rpm) in culture medium (IMDM/ 8%FCS/ 100U/ml penicillin/ 100µg/ml streptomycin) supplemented with 10ng/ml recombinant murine IL-7 (Peprotech) and retroviral supernatant. Transductions were performed in non-tissue-culture treated 24-wells plates that had been pre-coated with retronectin (TaKaRa) for at least 2h and thereafter blocked with 2%BSA in MQ for ½ h. Retroviral supernatants containing the barcode-library were generated as described[14] and diluted prior to use to reach a transduction efficiency of approximately 10%. One day after transduction, thymocytes were purified using Lympholite (Cedarlane) and GFP^{+} cells were sorted by FACS. 0.5-1.3x10^{6} sorted cells were injected intra-thymically into 4-6 weeks old primary (1°) recipient B6 mice, as described previously[15]. Additional pain relief (carprofen; 5 µg/g body weight; Pfizer) was given s.c. 1 day after the operation. 2-3 weeks after intra-thymic injections, CD8^{+} T cells were isolated from spleen and LNs (cervical, axillary, brachial, mesenteric, inguinal, lumbar) of 1° recipient mice by negative selection (Mouse CD8 T Lymphocyte Enrichment Set; BD Biosciences). Enriched CD8^{+} cells, containing barcode-labeled naïve T cells[15] were pooled from several 1° recipients and then transferred i.v. into several 8-10 weeks old B6 secondary (2°) recipients (400-1600 barcode-labeled cells / 2° recipient). This pooling and distribution approach guarantees that each 2° recipient receives an equal number of barcode-labeled T cells. Before injection, the fraction of GFP^{+} cells (typically ~0.01%) was determined by FACS to obtain an approximation of the number of transferred barcode-labeled T cells.

Listeria and influenza A infections. One day after receiving barcode-labeled naïve OT-I cells, 2° recipient mice were infected i.v. with a *Listeria monocytogenes* strain expressing chicken ovalbumin containing either the native SIINFEKL sequence (LM-OVA / LM-N4) or the altered peptide ligands SIIQFEKL (LM-Q4) or SIITFEKL (LM-T4) that are recognized with respectively ~18 and 71-fold lower avidity by OT-I T cells[22]. Unless stated otherwise, 2.5x10^{3} CFU *Listeria* were administered.

Alternatively, mice were anesthetized with ether and infected intra-nasally (i.n.) with 10[3] PFU of the recombinant influenza A/WSN/33 strain (Influenza-OVA) that expresses the H-2K[b]-restricted OVA$_{257-264}$ epitope[26]. T cell responses to infection were monitored in blood by FACS.

Recovery of barcode-labeled cells from infected mice. Barcode-labeled OT-I or OT-I rag2^{-/-} cells were recovered from spleen and LNs (cervical, axillary, brachial, mesenteric, inguinal, lumbar) of infected mice. To recover barcode-labeled spleen cells from living mice, partial splenectomy was performed as follows: Mice were anesthesized with isoflurane and the skin overlying the spleen was shaved and disinfected. A <1cm incision was made in the skin and peritoneum. ¼ of the spleen

was resected and the wound on the spleen was closed with Histoacryl® Topical Skin Adhesive (TissueSeal). Thereafter, peritoneum and skin were closed with ~3 stitches. Buprenorphine (0.1µg/g body weight; Schering-Plough) was given as pain relief 30 min. before and 6 h after the operation.

The isolated cells were subsequently enriched for $V\alpha2^+$ cells by MACS (Miltenyi Biotec; anti-PE Microbeads used after surface staining with $V\alpha2$-PE antibody) to facilitate efficient barcode recovery. To alleviate concerns that inter-group differences in total numbers and frequencies of barcode-labeled cells within the $V\alpha2$-enriched fraction might influence the efficiency of barcode amplification, the absolute number and percentage of GFP^+ cells being analyzed was adjusted between experimental groups. In practice, this meant that of the experimental group that induced a larger overall response, only a fraction of the isolated cells (harboring the same amount of GFP^+ cells as in the other group) was analyzed, after this sample had been topped with part of the previously removed $V\alpha2^-$ cells to adjust also the percentage of GFP^+ cells within the total cells being analyzed. In the experiment shown in Fig. 3, this adjustment occurred to the day 6 group, due to the small numbers of GFP^+ cells in the day 5 group. Of day 5 and 6, all GFP^+ cells were analyzed. All samples were stored as cell pellet at -80°C until barcode analysis.

The overall OT-I T cell response magnitude was determined by counting the number of GFP^+, $V\alpha2^+$ cells by flow cytometry within a small sample ($1/100^{th}$) taken from the MACS-enriched fraction. This counting occurred directly after MACS enrichment and before the adjustment of GFP^+ cell numbers and percentages.

Flow cytometry. Cell surface stainings were performed with the following reagents: $V\alpha2$-PE (B20.1), CD8-PerCp-Cy5.5 (53-6.7), CD8-APC (53-6.7)(BD Biosciences). Analyses were performed on a FACS Calibur (BD Biosciences) and analyzed with Summit v4.3 (Beckman Coulter) software. Cell sorting was carried out on a FACSAria Cell Sorter (BD Biosciences) or MoFlo Highspeed Sorter (Beckman Coulter).

Barcode amplification and second-generation sequencing. Genomic DNA was isolated from the frozen cell pellets using the DNeasy tissue kit (QIAGEN). Each sample was subsequently divided in two halves (sample A and B) that were independently amplified and analyzed further. This sample splitting serves as sampling control to test if barcodes could be representatively detected in the sample[3,11,14,15] and if amplification would introduce a bias in relative barcode abundance.

Barcode sequences were amplified by nested PCR, using top-LIB (5'-TGCTGCC-GTCAACTAGAACA-3') and bot-LIB (5'-GATCTCGAATCAGGCGCTTA-3') primers[14] in the first round (30 cycles: 5'' 94°C; 5'' 57.2°C; 5'' 72°C). In the experiment shown in Fig. 2D-F, the first round primers described previously[14] were used. The second round served to attach the P5 (5'- AATGATACGGCGACCACCGAGATCT-3') and P7 (5'- CAAGCAGAAGACGGCATACGAGAT-3') adaptors required for deep se-quencing on Illumina platforms, a sequencing primer annealing site ('seq_prim': 5'- ACACTCTTTCCCTACACGACGCTCTTCCGATCT-3') and a unique 6 bp index to the amplified barcode sequences. To enable multiplexing of several samples within

8

one sequencing lane, all 1st round PCR products of one sample were tagged with one of the 48 indices. All samples belonging to the same experiment were sequenced in the same lane. If the diversity of 48 index sequences and the number of samples per experiment allowed, multiple experiments were combined in one lane. Primers used in the second round PCR (30 cycles: 5'' 94°C; 5'' 57.2°C; 5'' 72°C) were according to the scheme: forward (5'-P7-seq_prim-index-CAGGCGCTTAGGATCC-3'), reverse (5'-P5-TGCTGCCGTCAACTAGAACA-3'). A list of the 48 index sequences is provided in Table S1. They were designed in a way that all indices differ by at least 2 bp, so that potential errors during amplification or sequencing leading to single-base changes within the index would not result in assignment of the read to a wrong sample.

After tagging all barcodes belonging to the same sample with a unique index, the second round PCR products of all samples meant for deep sequencing within the same lane were mixed at equal volumes. Subsequently, PCR products of the expected length (222bp) were purified from an e-gel (iBase, Invitrogen) and sequenced on GAIIx or HiSeq2000 platforms (Illumina). Total read lengths were 40 bp (GAIIx) or 50-60 bp (HiSeq2000), of which the first 22 bp consisted of the index and constant regions. The following 15 bp were used to distinguish between the different barcodes.

Controls in cellular barcoding experiments. To test whether the amount of template DNA per barcodes is large enough for reproducible barcode detection and quantification, in all experiments, each sample was divided in two half-samples that were independently amplified and sequenced (sampling controls[14]). A second essential control is the barcode distribution control[14], which tests the probability of two naïve T cells within the same mouse harboring the same barcode. If this would be the case, the progeny of these two founders could not be distinguished and would therefore faultily be analyzed as being one single family. The probability of such barcode sharing within the naïve T cell population can be estimated by determining the barcode overlap between two different mice[3,12-14].

Analysis of sequencing data. Sequence reads were first screened for quality by the software packages that are part of the Illumina pipeline and only high-quality reads were selected (~10-70x10^{6} per run). Next, only reads showing a 100% match to the expected scheme: index-CAGGCGCTTAGGATCC-random_sequence were selected (typically >90% of reads), whereby a 100% match to one of the 48 index sequences was required. Of the random sequence (the barcode), only the first 15 bp were considered. To filter out reads that reflect PCR or sequencing errors within the 15 bp barcode region, all remaining reads were compared to a barcode reference list, and only sequences that showed a 100% match to one of the listed sequences were selected (typically 80-93%). Subsequently, total read numbers per (half-)sample were normalized (always downscaled) to 100,000 reads, which enables direct comparison of read numbers per (half-)sample. As an additional way to reduce noise, all barcodes of which the average of the two corresponding half-samples represented <0.0005% of the total reads (<0.5 reads out of 100'000) were excluded from further analysis. This filtering step removed on average 0.04% of the remaining reads.

OT-I T cell family sizes are depicted either as percentage of the total response size or as absolute number of GFP+ (barcode-labeled) cells, obtained by multiplying the percentage of reads for a given barcode with the total number of GFP+ cells isolated.

If barcode abundance is presented in dot-plots, half-samples are depicted separately (sample A and B) and read counts of '0' are set to '0.05' to allow their visualization in log-scale plots. Original '0' values are used in all calculations.

To calculate the # of expected cells harboring a particular barcode (as done in Fig. S1), the total read number of all samples was normalized to 10,485,750 (=the total number of cells in the input sample).

Statistical analyses were performed using the 2-sided exact Wilcoxon test when 2 groups were compared and the 2-sided exact Jonckheere-Terpstra test when 3 groups were compared. Probabilities were considered significant if <0.05. Analyses were performed with Cytel Studio StatXact software.

Generation of the barcode reference list. To distinguish between barcode sequences that are present within the library and sequences that are the result of PCR or deep-sequencing errors, we created a barcode reference list by deep-sequencing the barcode-library twice. After normalizing the total number of reads between both samples, all sequences that were detected in both samples were sorted by frequency. A dominant sequence that constituted approximately 15% of total reads and thereby presumably reflected a bias introduced in original library generation was discarded, as the likelihood of random sharing between mice would be high. Likewise, sequences that deviated only 2bp from this barcode (and could therefore be the result of errors created during the PCR of this sequence) were removed from the list. In this analysis >40'000 sequences were observed, of which >90% were very infrequent (Fig. S8A). As sequence/ PCR errors are infrequent relative to the parental sequences, it should be possible to distinguish these by plotting the cumulative read number as a function of the number of sequences observed. As expected, we observed a steep change in the slope of the curve (indicating a substantial shift in the contribution subsequent barcodes made to the total pool of sequences), and only the highly prevalent sequences were present in both half samples at a ratio close to 1 (Fig. S8B). Sequences that cumulatively made up 92.5% of the reads (right of the vertical line in Fig. S8A+B) and those that were maximally 1.5-fold more prevalent in one of the two samples (two horizontal lines in Fig. S8B) were selected for the generation of the reference list. These cut-offs are chosen relatively stringent, so that library diversity might be slightly underestimated. In this way, a total of 2608 sequences were selected to constitute the barcode reference file. This is in line with the estimated size of the barcode-library, which was originally constructed from 4,743 clones[12] and is likely to have lost diversity during subsequent cloning steps.

ACKNOWLEDGEMENTS

REFERENCES

1. Obar, J. J., Khanna, K. M. & Lefrancois, L. Endogenous naive CD8+ T cell precursor frequency regulates primary and memory responses to infection. *Immunity* 28, 859-869 (2008).

2. Blattman, J. N. *et al*. Estimating the precursor frequency of naive antigen-specific CD8 T cells. *J. Exp. Med.* 195, 657-664 (2002).

3. van Heijst, J. W. *et al*. Recruitment of antigen-specific CD8+ T cells in response to infection is markedly efficient. *Science* 325, 1265-1269 (2009).

4. Murali-Krishna, K. *et al*. Counting antigen-specific CD8 T cells: a reevaluation of bystander activation during viral infection. *Immunity* 8, 177-187 (1998).

5. Butz, E. A. & Bevan, M. J. Massive expansion of antigen-specific CD8+ T cells during an acute virus infection. *Immunity* 8, 167-175 (1998).

6. Hasbold, J. *et al*. Quantitative analysis of lymphocyte differentiation and proliferation in vitro using carboxyfluorescein diacetate succinimidyl ester. *Immunol. Cell Biol.* 77, 516-522 (1999).

7. Gett, A. V. & Hodgkin, P. D. Cell division regulates the T cell cytokine repertoire, revealing a mechanism underlying immune class regulation. *Proc. Natl. Acad. Sci. U S A* 95, 9488-9493 (1998).

8. Veiga-Fernandes, H., Walter, U., Bourgeois, C., McLean, A. & Rocha, B. Response of naive and memory CD8+ T cells to antigen stimulation in vivo. *Nat. Immunol.* 1, 47-53 (2000).

9. Stoll, S., Delon, J., Brotz, T. M. & Germain, R. N. Dynamic imaging of T cell-dendritic cell interactions in lymph nodes. *Science* 296, 1873-1876 (2002).

10. Miller, M. J., Safrina, O., Parker, I. & Cahalan, M. D. Imaging the single cell dynamics of CD4+ T cell activation by dendritic cells in lymph nodes. *J. Exp. Med.* 200, 847-856 (2004).

11. Schumacher, T. N., Gerlach, C. & van Heijst, J. W. Mapping the life histories of T cells. *Nat. Rev. Immunol.* 10, 621-631 (2010).

12. Hawkins, E. D., Markham, J. F., McGuinness, L. P. & Hodgkin, P. D. A single-cell pedigree analysis of alternative stochastic lymphocyte fates. *Proc. Natl. Acad. Sci. U S A* 106, 13457-13462 (2009).

13. Stemberger, C. *et al*. A single naive CD8+ T cell precursor can develop into diverse effector and memory subsets. *Immunity* 27, 985-997 (2007).

14. Schepers, K. *et al*. Dissecting T cell lineage relationships by cellular barcoding. *J. Exp. Med.* 205, 2309-2318 (2008).

15. Gerlach, C. *et al*. One naive T cell, multiple fates in CD8+ T cell differentiation. *J. Exp. Med.* 207, 1235-1246 (2010).

16. Shendure, J. & Ji, H. Next-generation DNA sequencing. *Nat. Biotechnol.* 26, 1135-1145 (2008).

17. Voelkerding, K. V., Dames, S. A. & Durtschi, J. D. Next-generation sequencing: from basic research to diagnostics. *Clin. Chem.* 55, 641-658 (2009).

18. Kircher, M. & Kelso, J. High-throughput DNA sequencing--concepts and limitations. *Bioessays* 32, 524-536 (2010).

19. Zhou, X. *et al*. The next-generation sequencing technology and application. *Protein Cell* 1, 520-536 (2010).

20. Gerlach, C., van Heijst, J. W. & Schumacher, T. N. The descent of memory T cells. *Ann. N Y Acad. Sci.* 1217, 139-153 (2011).

21. Acuto, O. & Michel, F. CD28-mediated co-stimulation: a quantitative support for TCR signalling. *Nat. Rev. Immunol.* 3, 939-951 (2003).

22. Zehn, D., Lee, S. Y. & Bevan, M. J. Complete but curtailed T-cell response to very low-affinity antigen. *Nature* 458, 211-214 (2009).

23. Savage, P. A., Boniface, J. J. & Davis, M. M. A kinetic basis for T cell receptor repertoire selection during an immune response. *Immunity* 10, 485-492 (1999).

24. Trautmann, L. *et al*. Selection of T cell clones expressing high-affinity public TCRs within Human cytomegalovirus-specific CD8 T cell responses. *J. Immunol.* 175, 6123-6132 (2005).

25. Kedl, R. M., Kappler, J. W. & Marrack, P. Epitope dominance, competition and T cell affinity maturation. *Curr. Opin. Immunol.* 15, 120-127 (2003).

26. Topham, D. J., Castrucci, M. R., Wingo, F. S., Belz, G. T. & Doherty, P. C. The role of antigen in the localization of naive, acutely activated, and memory CD8(+) T cells to the lung during influenza pneumonia. *J. Immunol.* 167, 6983-6990 (2001).

SUPPLEMENTARY MATERIAL

Table S1: List of 48 index sequences.

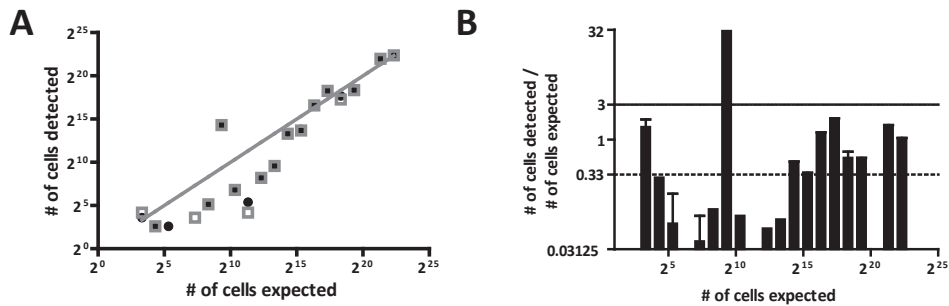| index number	index sequence						
1	ACACAG	13	TGCTAC	25	GTCAGT	37	CACATC
2	TCACGA	14	TGCTCT	26	GTCATG	38	CACAGA
3	TCAGCT	15	AGTGCT	27	GTCTAC	39	AGTGTC
4	ACAGTG	16	CACACT	28	GTCTCA	40	AGTCGA
5	TCGACT	17	CAGAGT	29	CTGTGT	41	AGTCAC
6	TCGAGA	18	CAGATG	30	CTGACA	42	AGCTGA
7	TCGATC	19	GATCGA	31	CTACGA	43	AGCATC
8	ACGTAG	20	CATCTG	32	CATGTC	44	AGAGCA
9	ACTCTG	21	GATGCT	33	CATCAC	45	ACTGAC
10	TGACTG	22	GTACAC	34	CAGTGA	46	ATACGC
11	TGAGAC	23	GTACTG	35	CAGTAC	47	ATAGCG
12	AGCACT	24	GTAGCA	36	CACTCA	48	ATCACG

8

Figure S1: Representative quantification of barcode abundances by deep sequencing. Two identical mixes of different cell numbers of single-barcode clones were analyzed by deep sequencing. The detected barcode frequencies were compared to the expected frequencies, which are based on the input number of cells. (**A**) Each dot represents one barcode in the first measurement and each square the second measurement. The line marks the position where the # of cells detected equals the # of cells expected. (**B**) Ratio between the detected and expected cell numbers per barcode.
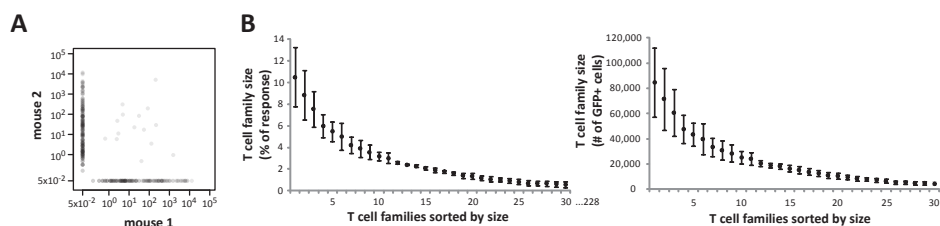
Figure S2: T cell responses are dominated by the progeny of few naïve T cells. Same experiment as depicted in Fig. 1. (**A**) Representative distribution control. The graph depicts the number of reads (out of 100'000) per detected barcode for 2 different mice. Each dot corresponds to one barcode. (**B**) Average OT-I T cell family sizes (+/- SD) of the largest 30 families out of an average total of 228 participating families.
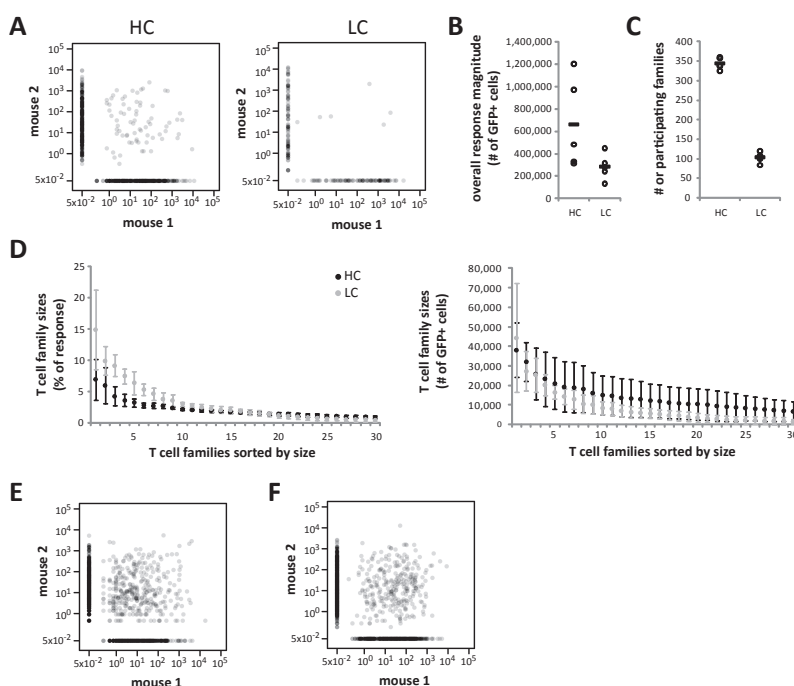
Figure S3: T cell family size disparity in OT-I rag2$^{-/-}$ T cell responses and as a function of naïve T cell frequency. (A-D) Same experiment as in Fig. 2A-C. HC: high cell numbers (760); LC: low cell numbers (190). (**A**) Representative distribution control. The graph depicts the number of reads (out of 100'000) per detected barcode for 2 different mice. Each dot corresponds to one barcode. (**B**) Overall response magnitude per group. Circles represent individual mice; bars averages. (**C**) Number of participating OT-I families per group. Circles represent individual mice; bars averages. (**D**) Average OT-I T cell family sizes (+/- SD) of the largest 30 families. (**E**) Same experiment as in Fig. 2D-F. Representative distribution control. On average 955 barcodes were detected. (**F**) Same experiment as in Fig. 2G-I. Representative distribution control. On average 804 barcodes were detected.
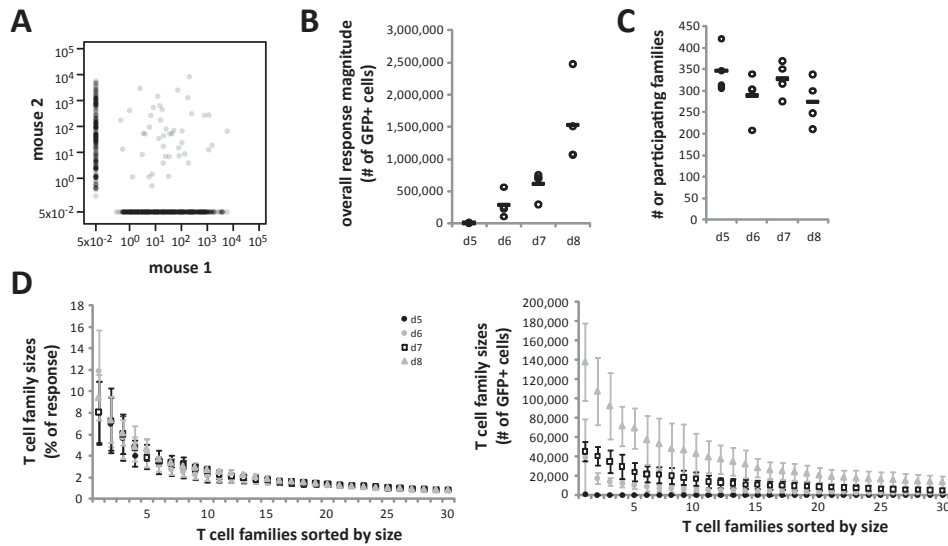
8

Figure S4: Differences in T cell family sizes are already observed early during the response. Same experiment as in Fig. 3. (**A**) Representative distribution control. The graph depicts the number of reads (out of 100'000) per detected barcode for 2 different mice. Each dot corresponds to one barcode. (**B**) Overall response magnitude per group. Circles represent individual mice; bars averages. (**C**) Number of participating OT-I families per group. Circles represent individual mice; bars averages. (**D**) Average OT-I T cell family sizes (+/- SD) of the largest 30 families.

A

mouse 2

10^5
10^4
10^3
10^2
10^1
10^0
5×10^{-2}

5×10^{-2} 10^0 10^1 10^2 10^3 10^4 10^5

mouse 1

B

overall response magnitude
(# of GFP+ cells)

1,400,000
1,200,000
1,000,000
800,000
600,000
400,000
200,000
0

wt   CD80/86$^{-/-}$

C

or participating families

600
500
400
300
200
100
0

wt   CD80/86$^{-/-}$

D

● wt
● CD80/86$^{-/-}$

T cell family sizes
(% of response)

30
25
20
15
10
5
0

5   10   15   20   25   30

T cell families sorted by size

T cell family sizes
(# of GFP+ cells)

140,000
120,000
100,000
80,000
60,000
40,000
20,000
0

5   10   15   20   25   30
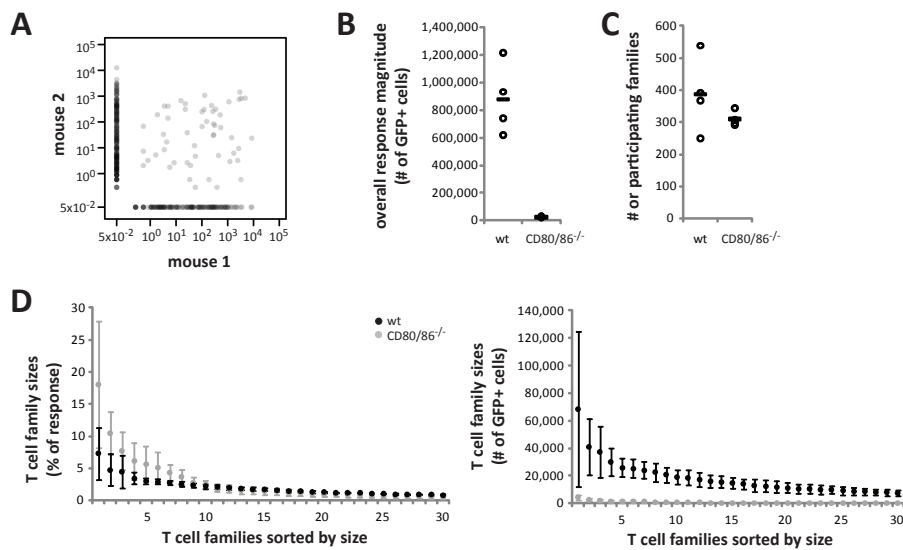
T cell families sorted by size

Figure S5: CD80/CD86-mediated costimulation influences the disparity in T cell family sizes. Same experiment as in Fig. 5. (**A**) Representative distribution control. The graph depicts the number of reads (out of 100'000) per detected barcode for 2 different mice. Each dot corresponds to one barcode. (**B**) Overall response magnitude per group. Circles represent individual mice; bars averages. (**C**) Number of participating OT-I families per group. Circles represent individual mice; bars averages. (**D**) Average OT-I T cell family sizes (+/- SD) of the largest 30 families.
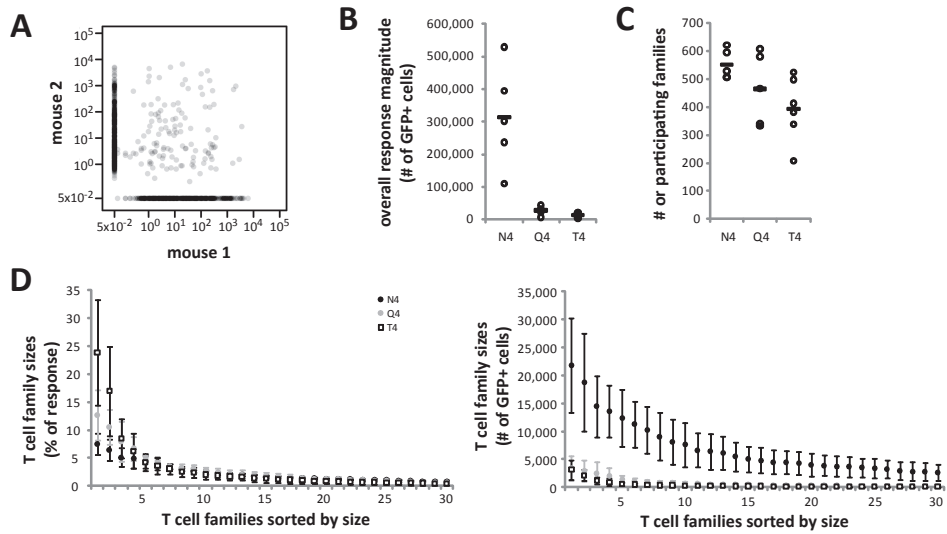
8

Figure S6: The dominance of a few T cell families is more pronounced in response to lower affinity antigens. Same experiment as in Fig. 5. (**A**) Representative distribution control. The graph depicts the number of reads (out of 100'000) per detected barcode for 2 different mice. Each dot corresponds to one barcode. (**B**) Overall response magnitude per group. Circles represent individual mice; bars averages. (**C**) Number of participating OT-I families per group. Circles represent individual mice; bars averages. (**D**) Average OT-I T cell family sizes (+/- SD) of the largest 30 families.
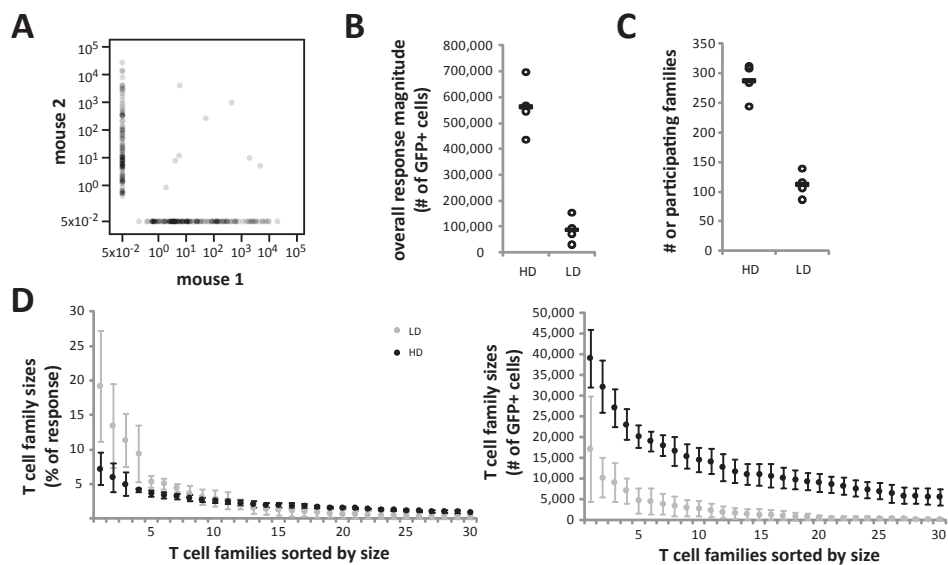
Figure S7: Lower antigen doses increase the inequality in T cell family sizes. Same experiment as in Fig. 5. HD: high dose (25'000 CFU); LD: low dose (500 CFU). (**A**) Representative distribution control. The graph depicts the number of reads (out of 100'000) per detected barcode for 2 different mice. Each dot corresponds to one barcode. (**B**) Overall response magnitude per group. Circles represent individual mice; bars averages. (**C**) Number of participating OT-I families per group. Circles represent individual mice; bars averages. (**D**) Average OT-I T cell family sizes (+/- SD) of the largest 30 families.
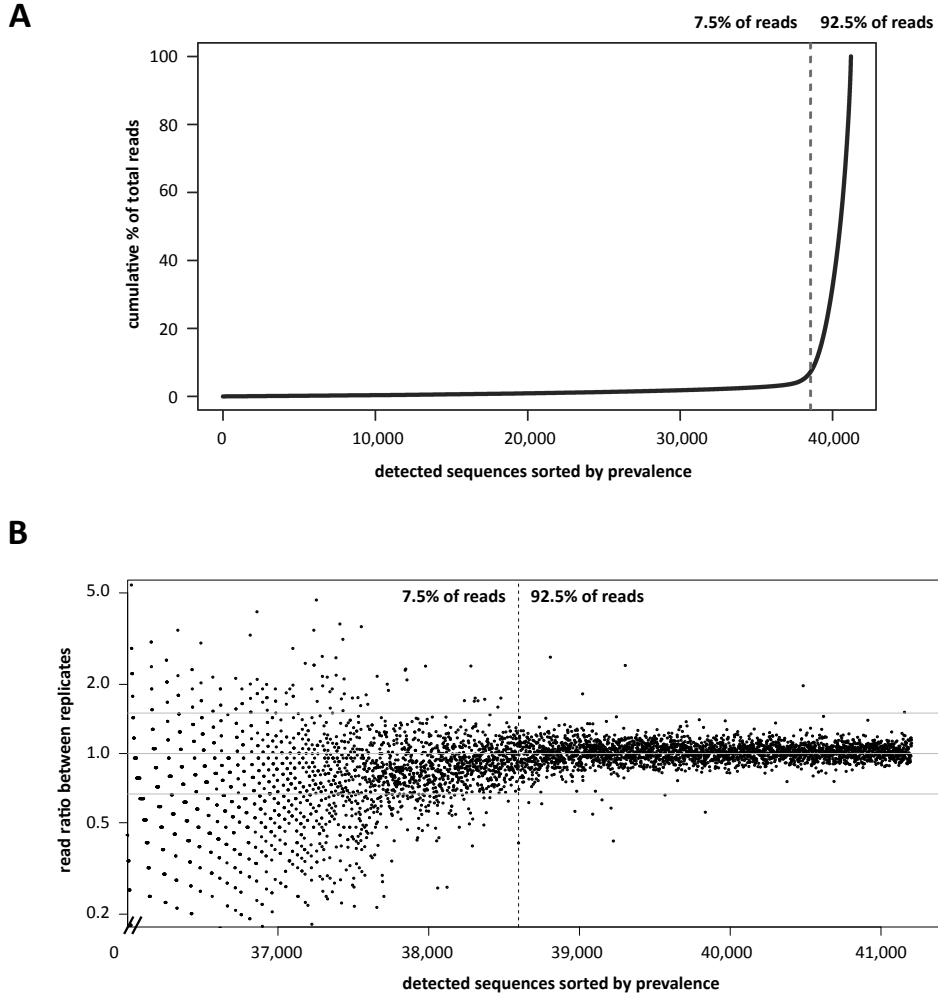
A

B

Figure S8: Generation of the barcode reference file. The barcode library was sequenced twice and the normalized reads of both samples are depicted. (**A**) Cumulative number of reads represented as a % of the total read count (100'000) per detected sequence. Vertical line represents the cut-off between 'noise' and 'real barcodes'. (**B**) Read ratio between both samples depicted per detected sequence. Each dot represents one detected sequence. Detected sequences are sorted by size and only the most prevalent ones are depicted (at least 36'000th position). The vertical line represents the cut-off between 'noise' and 'real barcodes'. The middle horizontal line indicates a read ratio of 1, the upper of 1.5 and the lower of 0.333. The outer two lines mark the second cut-off between 'noise' and 'real barcodes'.